



On the use of the similar media concept for scaling soil air permeability

Tiejun Wang, Xunhong Chen, Anh Minh A.M. Tang, Yu-Jun Cui

► To cite this version:

Tiejun Wang, Xunhong Chen, Anh Minh A.M. Tang, Yu-Jun Cui. On the use of the similar media concept for scaling soil air permeability. *Geoderma*, 2014, 235, pp.154-162. 10.1016/j.geoderma.2014.07.006 . hal-01086487

HAL Id: hal-01086487

<https://enpc.hal.science/hal-01086487>

Submitted on 26 Apr 2018

HAL is a multi-disciplinary open access archive for the deposit and dissemination of scientific research documents, whether they are published or not. The documents may come from teaching and research institutions in France or abroad, or from public or private research centers.

L'archive ouverte pluridisciplinaire **HAL**, est destinée au dépôt et à la diffusion de documents scientifiques de niveau recherche, publiés ou non, émanant des établissements d'enseignement et de recherche français ou étrangers, des laboratoires publics ou privés.

On the Use of the Similar Media Concept for Scaling Soil Air Permeability

Tiejun Wang^{1,*}

Xunhong Chen¹

Anh Minh Tang²

Yu-Jun Cui²

1. School of Natural Resources, University of Nebraska-Lincoln, Hardin Hall, 3310 Holdrege Street, Lincoln, Nebraska 68583, USA, 402-472-0772

2. Ecole des Ponts ParisTech, U.M.R. Navier/CERMES, 6 et 8, avenue Blaise Pascal, Cité Descartes, Champs-sur-Marne, 77455 Marne La Vallée cedex 2, France

Corresponding author: twang3@unl.edu

Revision submitted to *Geoderma*

Abstract

Soil air permeability (k_a) is an important factor that controls subsurface gas transport and exchange of gas across the soil-atmosphere interface. It is thus crucial to evaluate the spatial distribution of k_a for both application and modeling purposes. However, relevant studies are still very limited, partly due to the fact that the dependence of k_a on soil moisture levels cannot be directly included in the methods such as geostatistical techniques for analyzing the spatial distribution of k_a . To tackle this problem, the scaling scheme based on the similar media concept, which has been widely used in soil hydrology for characterizing spatial variability of soil hydraulic properties, was employed for scaling k_a in this study. Four air permeability models, including Millington and Quirk (1960)-MQ, Hunt (2005)-HT, Brooks and Corey (1964)-BC, and Kawamoto et al. (2006)-KA, were selected to test this method using two independent datasets. For the first dataset that included k_a measured for river sediments, all of the four models were able to delineate the spatial distribution of k_a with a reference curve of k_a and a set of scaling factors. Specifically, the MQ model gave the least satisfactory results due to the less flexibility of its form; whereas, there were no significant differences in the performances for the HT, BC, and KA models. For the second dataset that contained k_a measured for agricultural soils, the overall performance of the four models for scaling k_a deteriorated, largely due to the alterations in the microscopic structures of soil samples caused by repacking and compression of soil samples. Nonetheless, as the first attempt, this study shows the viability of using the similar media concept for scaling k_a . The merit of this method resides in the fact that the spatial variations of moisture conditions and soil properties can be simultaneously included for analyzing the spatial distribution of k_a . With a reference curve of k_a and the distribution of scaling factors, this method would be particularly suitable for modeling subsurface gas transport.

Keywords: Similar Media Concept, Scaling Factor, Soil Air Permeability, Air Permeability Model

1. Introduction

As one of the key factors that control subsurface gas transport and exchange of gas across the soil-atmosphere interface, soil air permeability (k_a) describes the ability of a soil to transmit gas. The rising interest in k_a is manifested by its broad range of applications in various fields, including greenhouse gas emission (Ball et al., 1997; Conen et al., 1998), landfills (Jain et al., 2005; Wu et al., 2012), soil vapor extraction systems (Poulsen et al., 1998; Farhan et al., 2001), crop growth (Lipiec and Hatano, 2003; Barrios et al., 2005). Moreover, due to easy operation and cost effectiveness, k_a measured near field capacity has been used to predict soil saturated hydraulic conductivity (Loll et al., 1999; Iversen et al., 2001).

Under natural conditions, k_a is affected by a number of soil factors (e.g., air-filled porosity and pore size distribution) and moisture conditions, all of which show various degrees of spatial variations. As such, field measured k_a exhibits significant spatial variability (Iversen et al., 2003). For application and modeling purposes, it is thus crucial to evaluate the spatial distribution of k_a and its controlling factors. However, compared to relevant researches on soil hydraulic properties, only few studies are available on the spatial distribution of k_a , which nonetheless provided valuable insights into the understanding of the spatial pattern of k_a (Poulsen et al., 2001; Iversen et al., 2003, 2004). Geostatistical techniques were mainly used in previous studies to analyze the spatial pattern of k_a . Based on the results of variograms, Iversen et al. (2003) found that the range of k_a for sandy soils was larger than the one for a loamy soil, probably due to the difference in the depositional processes of those two types of soils. Although geostatistical techniques have been proven to be powerful tools for investigating naturally occurred phenomena, there are certain shortcomings for those techniques as pointed out by Henley (2001). Most notably, the underlying processes associated with studied targets cannot be explicitly considered in geostatistical techniques, which rather rely on statistical models for examining the spatial correlations of the targets.

With respect to k_a , the main issue of using geostatistical techniques stems from the impact of soil moisture on k_a . It has been well known that k_a is highly dependent on soil moisture levels, but the spatial distribution of soil moisture cannot be directly included in the geostatistical analyses of k_a . To some degree, this is analogous to study the spatial distribution of soil unsaturated hydraulic conductivity without specifying moisture conditions. Therefore,

precautions were usually taken in previous field studies on the spatial distribution of k_a . As conjectured by Iversen et al. (2003), when soil moisture contents reach field capacity, the air flow takes place in the majority of soil pores; thus, the impact of moisture on k_a can be neglected with moisture contents near and below field capacity. Although the assumption made by Iversen et al. (2003) is useful for studying the spatial distribution of k_a under dry conditions, it may fail at regions with wet climates or shallow groundwater tables. For application purposes (e.g., landfills and soil vapor extraction systems), the inclusion of moisture in analyzing the spatial distribution of k_a is also inevitable. Therefore, it is desirable to seek alternative methods to assess the spatial distribution of k_a under the influence of soil moisture.

Along the line of above thinking, the scaling scheme based on the similar media concept may provide a promising approach to investigating the spatial distribution of k_a with the consideration of moisture conditions. First introduced by Miller and Miller (1956), the similar media concept is based on the assumption that the internal geometry of similar media only differs by microscopic length scales that can be characterized by scaling factors. The purpose of this scaling approach is to coalesce a range of functional relationships into a single curve through scaling factors that depict the spatial distribution of those functional relationships. More specifically, scaling factors are used to relate soil properties at a given location to the mean properties at a reference location, which are invariant of moisture conditions. This scaling method has been widely used in soil hydrology to characterize spatial variability of soil hydraulic properties and soil hydraulic functions with associated model parameters (Warrick et al., 1977; Hopmans, 1987; Shouse and Mohanty, 1998; Zavattaro et al., 1999; Hendrayanto et al., 2000; Tuli et al., 2001). With a reference functional relationship and the distribution of scaling factors, this method is particularly suitable for modeling purposes (Peck et al., 1977; Kabat et al., 1997; Salvucci, 1998; Oliveira et al., 2006). Given the similarities between water flow and gas transport in soils, one can expect the viability of applying this scaling approach for investigating the spatial distribution of k_a under the influence of soil moisture.

To our knowledge, this research was the first attempt to extend the use of the similar media concept for scaling k_a . The main objective of this study was to examine the feasibility of this approach using two datasets collected from USA and France. Four air permeability models were selected to delineate the functional relationship between k_a and saturation degree of air. The

results of this study demonstrated the feasibility of using the similar media concept for scaling k_a , which also opened the door for utilizing this method for simulating gas transport in soils.

2. Materials and Methods

2.1 Similar Media Concept in Soil Hydrology

The use of the similar media concept for scaling soil water retention and hydraulic conductivity curves is well documented in the literature (see the review by Vereecken et al., 2007). So, only a brief overview is given here. Based on the similar media concept, it is assumed that the microscopic structures (e.g., tortuosity, and relative particle size and pore size distributions) of similar soils are identical and only differ by microscopic length scales that can be characterized by scaling factors (Peck et al., 1977; Warrick et al., 1977). The scaling factor (α) is thus defined by the ratio of the microscopic characteristic length of a soil (λ) to the characteristic length of a reference soil (λ_m):

$$\alpha_i = \frac{\lambda_i}{\lambda_m} \quad (1)$$

where $i=1, 2, \dots, L$ is the location of the soil and the subscript m denotes the reference soil. By its definition, α is invariant of soil moisture conditions and only dependent upon the location of the soil. As such, the soil water retention curve at any location can be scaled to the reference water retention curve through α :

$$h_i(\theta) = \frac{h_m(\theta)}{\alpha_{w,i}} \quad (2)$$

where h is the soil matric potential, θ is the volumetric moisture content, and the subscript w denotes water. The scaling relationship of the soil hydraulic conductivity curve can be written as:

$$K_{w,i}(\theta) = K_{w,m}(\theta) \alpha_{w,i}^2 \quad (3)$$

where K_w is the hydraulic conductivity. Due to the fact that soil porosity may vary across locations, instead of θ , the saturation degree of moisture (S_w) is usually used (Warrick et al., 1977):

$$S_w = \frac{\theta}{\phi} \quad (4)$$

where ϕ is the soil porosity.

To describe the reference curves of h_m and $K_{w,m}$, soil water retention and hydraulic conductivity models (e.g., Brooks-Corey model and van Genuchten model) have been used, although polynomial functions of $h_m(S_w)$ and $K_{w,m}(S_w)$ were also adopted (Warrick et al., 1977). By optimizing the differences between measured and calculated $h(S_w)$ and $K_w(S_w)$ across all the locations, the model parameters for the reference curves of h_m and $K_{w,m}$, and the scaling factor $\alpha_{a,i}$ at each location can be obtained (Hopmans, 1987; Tuli et al., 2001).

2.2 Extension of the Similar Media Concept for Scaling Soil Air Permeability

Although the scaling theory based on the similar media concept has been widely used in soil hydrology, there is a surprising lack of studies on its application for assessing the spatial distribution of k_a . Strictly speaking, soil water permeability (k_w) should be used in the scaling procedure (Eq. (3)), as regardless of fluid properties, soil permeability, whether it is k_w or k_a , represents the intrinsic properties of soils to transmit fluids and thus reflects the microscopic structures of soils. However, given that the fluid of interest remains under the same conditions (e.g., temperature), the fluid properties do not change across locations and conductivities (e.g., K_w) can be used in Eq. (3). Therefore, one can write a similar scaling relationship for k_a based on Eq. (3):

$$k_{a,i}(S_a) = k_{a,m}(S_a) \alpha_{a,i}^2 \quad (5)$$

where $S_a = (1 - S_w)$ is the saturation degree of air and the subscript a denotes air. For the same reason for using S_w in scaling $h(S_w)$ and $K_w(S_w)$, S_a was used in this study instead of the volumetric soil-air content. Note that α_a is also invariant of soil moisture conditions and only dependent upon the location of the soil.

To delineate the reference relationship of $k_{a,m}$, four air permeability models were selected (Ghanbarian-Alavijeh and Hunt, 2012). The first model was proposed by Millington and Quirk (1960) (denoted as MQ hereafter):

$$k_a(S_a) = k_o \times S_a^2 \quad (6)$$

where k_o is the air permeability at the porosity ϕ .

The second model was developed by Hunt (2005) (HT), which is based on the continuum percolation theory:

$$k_a(S_a) = k_o \left(\frac{S_a - S_{a,t}}{1 - S_{a,t}} \right)^2 \quad (7)$$

where $S_{a,t}$ is the percolation threshold used by Ghanbarian-Alavijeh and Hunt (2012). Note that the HT model can be reduced to Eq. (6) by assuming $S_{a,t}=0$.

The third model was based on the hydraulic conductivity function of Brooks and Corey (1964) (BC):

$$k_a(S_a) = k_o S_a^l \left[1 + (1 - S_a)^{1+\frac{2}{\gamma}} \right] \quad (8)$$

where γ is the pore size distribution index, and l is the tortuosity-pore connectivity factor and assumed to be 2 based on the percolation theory (Hunt and Ewing, 2009).

The last model was taken from Kawamoto et al. (2006) (KA):

$$k_a(S_a) = k_o \times (S_a)^{1+3/\eta} \quad (9)$$

where $(1+3/\eta)$ represents the combined effects of tortuosity and connectivity of air-filled pores. In Kawamoto et al. (2006), the measured k_a at -100 cm H₂O was used instead of k_o . Essentially, the MQ model is a simplified version of Eq. (9) with $\eta=3$.

In parallel to previous studies on scaling $h(S_w)$ and $K_w(S_w)$, the scaling factors $\alpha_{a,i}$ and the model parameters (given in Tables 2 and 3) for describing the reference curves of $k_{a,m}$ were obtained by optimizing the differences between measured and calculated k_a . The following objective function was used:

$$O = \sum_{i=1}^L \left\{ \sum_{j=1}^{M(i)} \left[k_{a,i}^{obs}(S_{a,j}) - \alpha_{a,i}^2 \times k_{a,m}(S_{a,j}) \right]^2 \right\} \quad (10)$$

where $M(i)$ is the total number of observed k_a at location i , $k_{a,i}^{obs}(S_{a,j})$ is the j th observed k_a corresponding to $S_{a,j}$ at location i , and $k_{a,m}(S_{a,j})$ is the calculated k_a at $S_{a,j}$ from Eq. (6) to Eq.(9).

The generalized reduced gradient method was used to optimize Eq. (10) with the geometric mean of the scaling factors assumed to be unity (Hopmans, 1987; Zavattaro et al., 1999; Hendrayanto et al., 2000):

$$(\prod_{i=1}^L \alpha_i)^{1/L} = 1 \quad (11)$$

To evaluate the performance of each air permeability model, the root mean square error (RMSE) was used:

$$RMSE = \left(\frac{1}{n} \sum_{k=1}^n (o_k - e_k)^2 \right)^{\frac{1}{2}} \quad (12)$$

where n is the total number of observed k_a across all the locations, o_k is either observed $k_{a,i}(S_{a,j})$ or scaled $k_{a,i}(S_{a,j})$ (i.e., observed $k_{a,i}(S_{a,j}) \times \alpha_{a,i}^2$), and e_k is the corresponding $k_{a,m}(S_{a,j})$ calculated from the reference curve of $k_{a,m}$.

2.3 Datasets

Two independent datasets collected from USA and France were used in this study to test the feasibility of applying the similar media concept for scaling k_a . The first dataset (denoted as Dataset I) included measured air permeability data using sediment samples taken from the channel of the Platte River near Kearney, NE (Figure 1). The streambed sediments at the site are moderately-sorted, and mainly consist of sands and gravels with very low organic matter contents (Table 1). A total of 25 samples with a length of 20 cm for each sample were collected using transparent polycarbonate tubes with an inside diameter of 5.1 cm. The tubes were vertically pressed to the depth of 20 cm into the sediments. The distance between neighboring sampling locations was 1 m. After taking out the sample from the river channel, the bottom of the tube was wrapped by a fiberglass screening to prevent sediments from falling off. A falling head permeability test was carried out on site to determine the saturated hydraulic conductivity of the sediments inside the tube (Chen, 2005). Water temperatures were also recorded during the test to calculate water dynamic viscosity, which was used to calculate k_w .

After the measurements of saturated hydraulic conductivities, the sediment samples were brought back to the laboratory and air dried at room temperatures. On Day 2 and every three

days afterwards until Day 17, air permeability tests were performed using a portable air permeameter (Figure 2), which resulted in 6 pairs of data points of k_a and S_a for each tested sample. To measure k_a , the polycarbonate tubes were connected to the air permeameter, which mainly consisted of an air tank, an air pressure regulator, a rotameter that measured the flow rate of air through the sediments, and a manometer that recorded the pressure difference across the length of the sediments. Darcy's Law was then used to calculate k_a (Kirkham, 1947). Due to the slippage of gas molecules near the pore wall, the flow of gas in porous media may exhibit non-Darcian flow that leads to higher k_a (Klinkenberg, 1941). Therefore, additional tests were performed to examine the applicability of Darcy's Law by measuring the pressure difference across the sample length under varying flow rates. The linearity of the results proved the applicability of Darcy's Law and confirmed the air permeameter was operational for measuring k_a . The merit of the air permeameter used in this study is that it allows to measure both saturated hydraulic conductivity and k_a of the same sample without the need to remove the sediments from the permeameter for repacking. Thus, it minimizes the possible disturbance of the sample structure. After each air permeability test, samples were immediately weighed to determine moisture contents and corresponding volumetric soil-air contents. On Day 17, all of the samples were dried in the oven for 24 h at the temperature of 105 °C to determine bulk density and porosity. The results of the grain size analyses showed that the texture of the sediments was sand according to the USDA classification (Table 1).

The second dataset (denoted as Dataset II) was taken from Tang et al. (2011) and contained nine remolded soil samples from an experimental forest site at Le Breuil located in central France. The reason for choosing Dataset II was that several air permeability models, including the HT model, were successfully tested on those soil samples (Tang et al., 2011; Ghanbarian-Alavijeh and Hunt, 2012). However, unlike the air permeameter used in Dataset I, a specially designed oedometer was adopted by Tang et al. (2011) to measure $k_a(S_a)$ by vertically compressing soil samples, which led to varying moisture contents under different compressional stresses. Except for one sample with 6 data points, there were 8 pairs of k_a and S_a for each sample. The texture of the soils was sandy loam and their physical properties are reported in Table 1.

3. Results and Discussions

3.1 Dataset I

It has been well known that besides soil properties, k_a is also affected by moisture conditions and thus S_a . With the drying process, the mean value of S_a for Dataset I increased from 0.49 on Day 2 to 0.87 on Day 17. Consequently, the mean value of k_a was almost quadrupled from 21.0 μm^2 on Day 2 to 83.6 μm^2 on Day 17, as more smaller pores opened up for transmitting air when the sediments became drier. The results from Dataset I again illustrate the importance of including moisture conditions in analyzing the spatial distribution of k_a . To further demonstrate the impact of S_a on k_a , the results from four sediment samples in Dataset I (numbered as #1, #2, #3, and #4) are plotted in Figure 3. As expected, k_a increased with increasing S_a or with decreasing moisture levels; however, the $k_a(S_a)$ relationship also differed among different samples. More specifically, k_a showed similar ranges for #1 (13.7 to 41.5 μm^2) and #2 (13.2 to 44.5 μm^2) with S_a ranging from 0.40 to 0.81 and 0.56 to 0.86, respectively (Figures 3a and 3b). In comparison, k_a for #3 (11.3 to 142.3 μm^2) and #4 (4.5 to 111.5 μm^2) varied over an order of magnitude with S_a increasing from 0.46 to 0.90 and 0.42 to 0.89, respectively (Figures 3c and 3d). Clearly, a single curve of $k_a(S_a)$ is not sufficient to describe spatially distributed k_a , even at plot scales (e.g., a reach scale in this study). This presents a great challenge for simulating subsurface gas transport with spatially varied k_a and associated model parameters. The same challenge is also faced by soil hydrologists to simulate water movement in vadose zone, where soil hydraulic properties may vary substantially across landscapes. One of the solutions to tackle this problem in soil hydrology relies on the use of scaling factors within the framework of the similar media concept (Kabat et al., 1997; Salvucci, 1998; Oliveira et al., 2006).

To have a thorough view of the effectiveness of using the similar media concept for scaling k_a , the results of unscaled and scaled k_a from Dataset I are plotted in Figure 4 with the reference curves of $k_{a,m}$ for all of the air permeability models. For the purpose of clarity, the results of scaled k_a for each model are also plotted separately in Figure 4. The scaled k_a was calculated using the obtained scaling factors (e.g., Eq. (5)). The obtained fitting parameters and RMSE values for each model are given in Table 2. Note that the results of two sediment samples were removed from the analyses, as they exhibited irregular patterns between k_a and S_a (e.g., k_a may decrease with increasing S_a). Those irregular patterns were suspected to be the consequence of

the collapse of root holes in the samples during the drying process. As expected, a positive trend existed between unscaled k_a and S_a . When S_a was lower than 0.7, unscaled k_a largely remained below $60 \mu\text{m}^2$, while unscaled k_a varied about 8 times from approximately 20 to $160 \mu\text{m}^2$ when S_a reached above 0.8. Figure 5a further shows that a single curve of $k_a(S_a)$ is not sufficient to delineate the distribution of the unscaled k_a as attested by the $k_{a,m}$ curves. By comparison, with the aid of scaling factors, the scaled k_a coalesced along the $k_{a,m}$ curves with greatly reduced scatter for all of the four air permeability models. Note that scaled k_a was systematically more scattered at the lower range of S_a for all of the models. It was due to the fact that more weights were given to higher values of k_a in Eq. (10) during the optimization process. If k_a was replaced by $\log k_a$ in Eq. (10), the scatter of scaled k_a at the lower range of S_a could be reduced; however, the overall performance of the models deteriorated. Compared to the other three $k_{a,m}$ curves, the one for the HT model slightly deviated; whereas, the resulting scaled k_a was comparable for all of the four models (Figure 4b). Among all of the results, the RMSE value of the scaled k_a for the MQ model was highest with $k_{a,m}$ overestimating scaled k_a at the lower end of S_a and underestimating scaled k_a at the higher end of S_a (Figure 4c). This was because without additional fitting parameters other than k_o , the form of the MQ model was the least flexible. By contrast, the performances of the other three $k_{a,m}$ curves improved at both ends of S_a with the BC model showing the most satisfactory results (Figures 4d-4f); however, there appeared no significant differences in the performances of those three air permeability models for scaling k_a (Table 2), indicating the applicability of those models for delineating the distribution of k_a in the studied sediments.

The values of obtained k_o varied among the four models (Table 2). The fitted k_o in the KA model was highest with the value of $106.0 \mu\text{m}^2$, while the one in the MQ model was only $92.5 \mu\text{m}^2$. As a result, the scaled k_a for the MQ model was lowest under the same level of S_a ; however, the differences in the scaled k_a were minimum among different models. The value of the obtained percolation threshold $S_{a,t}$ in the HT model was 0.168, which was comparable to the 0.1 threshold proposed by Ewing and Hunt (2006). In addition, the pore size distribution index γ ($\gamma = 3.067$ in this study) in the BC model fell within the range for sandy soils (Ghanbarian-Alavijeh and Hunt, 2012). In summary, Figure 4 shows that for the studied sediments, the spatially distributed k_a could be described by a reference curve of $k_{a,m}$ and a set of scaling factors, which attests the feasibility of using the similar media concept for scaling k_a under the influence of

moisture. With a known reference curve of $k_{a,m}$ and the distribution of scaling factors, this method would be particularly suitable for modeling subsurface gas transport.

As previously explained, the spatially distributed k_a is mostly controlled by moisture conditions and soil properties, both of which may vary at different spatiotemporal scales. Essentially, the impacts of moisture levels and S_a on k_a can be determined through the reference curve of $k_{a,m}$; whereas, the spatial variations of soil properties are embedded in the distribution of scaling factors, as scaling factors only depend on soil intrinsic properties (i.e., the microscopic characteristic length). The probability plots of the scaling factors (both $\alpha_{a,i}$ and $\ln\alpha_{a,i}$) are given in Figure 5 for the HT model. The resulting probability plots were similar for all of the four models, so only the ones for the HT model are presented here. The respective mean and standard deviation was 1.03 and 0.23 for $\alpha_{a,i}$, and 0 and 0.23 for $\ln\alpha_{a,i}$. The values of the standard deviations for $\alpha_{a,i}$ and $\ln\alpha_{a,i}$ were smaller than previously reported values derived from soil water retention and hydraulic conductivity data (Warrick et al., 1977; Hopmans, 1987; Hendrayanto et al., 2000), probably due to the smaller number of sediment samples used in this study. Although those previous studies showed a log normal distribution of scaling factors, the Kolmogorov-Smirnov Test did not reject the null hypothesis that $\alpha_{a,i}$ and $\ln\alpha_{a,i}$ were normally distributed at the significance level of 0.01. Thus, future studies are needed to include a larger number of samples, and to compare the distributions of scaling factors drawn separately from soil water retention and hydraulic conductivity data and from air permeability data.

To test the applicability of the derived reference curves of $k_{a,m}$, the values of k_a on Day 17 were calculated using the obtained scaling factors and measured S_a based on Eq. (5). As hypothesized by Iversen et al. (2003), when soil moisture contents reach field capacity, the air flow takes place in the majority of soil pores; thus, k_a measured at or near field capacity can be used as a proxy of soil water permeability k_w to predict saturated hydraulic conductivity. On Day 17, the average value of soil moisture contents for all of the sediment samples was 0.04, which was quite comparable to the observed field capacity of sandy soils (soil moisture data can be accessed from the High Plains Regional Climate Center at <http://www.hprcc.unl.edu/awdn/soilm/>). Based on the above reasoning, the calculated k_a on Day 17 is plotted against k_w derived from measured saturated hydraulic conductivities in Figure 6. Again, only the calculated k_a for the HT model is shown here as a demonstration. It can be seen

from Figure 6 that the calculated k_a was very close to k_w . On average, the calculated k_a only underestimated k_w by 11%. Figure 6 further corroborates the feasibility of using scaling factors within the similar media framework for describing spatially distributed k_a .

3.2 Dataset II

The previous section has demonstrated the feasibility of using the similar media concept for scaling k_a in river sediments. To assess the viability of this method in agricultural soils, analyses were carried out for Dataset II. A mean value of 0.02 for $S_{a,t}$ in the HT model was obtained by Ghanbarian-Alavijeh and Hunt (2012) by fitting individual curves of k_a to soil samples in Dataset II. Thus, to avoid the negative values of $(S_a - S_{a,t})$ in Eq. (7), $S_{a,t}$ was fixed to be 0.02 for Dataset II. In addition, an unusually high value of γ in the BC model was obtained from the optimization, which was caused by fitting the $k_{a,m}$ curve to comparatively low values of k_a from one soil sample (the data points with S_a between 0 and 0.2 shown in Figure 7a). Moreover, no physical constraints for the fitting parameters were considered in the optimization process and $k_a(S_a)$ in Eq. (8) became insensitive to γ for large γ values. Thus, instead of using this high value of γ , the class-averaged value of γ for sandy loam was used, which was derived from soil water retention data (Rawls et al., 1982).

The unscaled and scaled k_a from Dataset II are presented in Figure 7, and the obtained fitting parameters and RMSE values are given in Table 3. Overall, the unscaled k_a from Dataset II exhibited a much wider distribution from 0.5 to 1980.8 μm^2 . Some of the remolded samples (e.g., the one with the maximum k_a of 1980.8 μm^2) also showed different ranges of k_a (Figure 7a), which was probably caused by the repacking processes. As expected, the improvement of the scaled k_a from the MQ model was least satisfactory (Figure 7c). By comparison, the performances of the HT and BC models were considerably improved; however, the obtained $k_{a,m}$ tended to overestimate most of the scaled k_a (Figures 7d and 7e), owing to the fact that the fitting parameter (or shape factor) $S_{a,t}$ in the HT model and γ in the BC model were fixed during the optimizations. Without the need to fix the fitting parameter η in the KA model, the $k_{a,m}$ curve seemed to more reasonably delineate the distribution of the scaled k_a over the entire range of S_a (Figures 7f), although it should be noted that a very high value of k_o was obtained for the KA

model in order to match the data points from the sample with the maximum k_a of $1980.8 \mu\text{m}^2$. Using the same remolded samples from Dataset II, Ghanbarian-Alavijeh and Hunt (2012) showed that the HT model was better than the other three models (e.g., MQ, BC, and KA) to describe the $k_a(S_a)$ relationship for individual samples; however, no significant improvement of the HT model was found in this study for scaling k_a . One of the possible reasons for the different conclusions about the model performances was due to the differences in the optimization procedures. In Ghanbarian-Alavijeh and Hunt (2012), the $k_a(S_a)$ curves were optimized for individual samples and some of the fitting parameters (e.g., γ in the BC model) were obtained through optimizing soil retention data rather than soil permeability data.

In comparison to the results from Dataset I, the overall performance of the four selected air permeability models for scaling k_a was less satisfactory for Dataset II, which can be attributed to two reasons. First, for the soil samples in Dataset II, soil structures might have been altered during the repacking processes. Secondly, in order to achieve different moisture levels, soil samples were compressed using an oedometer (Tang et al., 2011), which unavoidably changed the microscopic structures of soils. The repacking processes and the compression of soil samples might have led to variations in the microscopic structures among different soil samples and thus the less satisfactory performance of using the similar media concept for scaling k_a . Nonetheless, Figure 7 shows that the use of scaling factors was able to narrow down the scatter of k_a around the $k_{a,m}$ curves for the HT, BC, and KA models. In terms of the distribution of scaling factors from Dataset II, the respective mean and standard deviation for the HT model was 1.01 and 0.14 for $\alpha_{a,i}$, and 0 and 0.13 for $\ln\alpha_{a,i}$. Again, the values of the standard deviations for $\alpha_{a,i}$ and $\ln\alpha_{a,i}$ were smaller than the previously reported values derived from soil water retention and hydraulic conductivity data (Warrick et al., 1977; Hopmans, 1987; Hendrayanto et al., 2000).

4. Conclusions

The use of the scaling factors based on the similar media concept was tested for scaling air permeability k_a using two independent datasets in this study. With a reference curve of $k_{a,m}$ and a set of scaling factors, this method was shown to be able to delineate the spatial distribution of k_a for the first dataset, which included k_a measured under different moisture conditions by drying river sediment samples. For the second dataset that contained k_a measured for agricultural soils,

however, the use of the similar media concept for scaling k_a was less successful. It was most likely due to the alterations in the microscopic structures of soil samples caused by repacking and compression of soil samples. The merit of this method resides in the fact that the spatial variations of moisture conditions and soil properties can be simultaneously included for analyzing the spatial distribution of k_a . At any given location, the impact of S_a and thus moisture levels on k_a can be quantified by the reference curve of $k_{a,m}$; whereas, soil properties are embedded in the scaling factors. Since this study was the first attempt to apply the similar media concept for scaling k_a , more studies are needed to test this method on soils with different textures and to examine the impacting factors that control the distribution of scaling factors. It would be also useful to compare scaling factors derived independently from air permeability data, and from soil water retention and hydraulic conductivity data, which may further elucidate the physical meanings of those scaling factors. Future studies are also needed to incorporate this method in modeling subsurface gas transport.

Acknowledgements

Iain Nicolson Audubon Center at the Rowe Sanctuary in Nebraska allowed the authors to access the Platte River channel for collecting streambed cores and conducting permeameter tests. The authors would like to thank P. Hanson of University of Nebraska-Lincoln for providing assistance in the lab analyses. The research was partially supported by National Basic Research Program of China (2014CB744700).

References

- Ball BC, Dobbie KE, Parker JP, Smith KA. 1997. The influence of gas transport and porosity on methane oxidation in soils. *Journal of Geophysical Research* **102**: 23301–23308.
- Barrios E, Cobo JG, Rao IM, Thomas RJ, Amezquita E, Jimenez JJ, Rondon MA. 2005. Fallow management for soil fertility recovery in tropical Andean agroecosystems in Colombia. *Agriculture, Ecosystems & Environment* **110**: 29–42.
- Brooks RH, Corey AT. 1964. Hydraulic properties of porous media. *Hydrol. Pap. 3*. Dep. of Civ. Eng., Colo. State Univ., Fort Collins.
- Chen XH. 2005. Statistical and geostatistical features of streambed hydraulic conductivities in the Platte River, Nebraska. *Environmental Geology* **48**: 693–701.
- Conen F, Smith KA. 1998. A re-examination of closed flux chamber methods for the measurement of trace gas emissions from soils to the atmosphere. *European Journal of Soil Science* **49**: 701–707.
- Ewing R, Hunt A. 2006. Dependence of the electrical conductivity on saturation in real porous media. *Vadose Zone Journal* **5**: 731–741. DOI:10.2136/vzj2005.0107.
- Farhan S, Holsen TM, Budiman J. 2001. Interaction of soil air permeability and soil vapor extraction. *Journal of Environmental Engineering* **127**: 32– 37.
- Ghanbarian-Alavijeh B, Hunt AG. 2012. Comparison of the predictions of universal scaling of the saturation dependence of the air permeability with experiment. *Water Resources Research* **48**: W08513. DOI:10.1029/2011WR011758.
- Hendrayanto, Kosugi K, Mizuyama T. 2000. Scaling hydraulic properties of forest soils. *Hydrological Processes* **14**: 521–538.
- Henley S. 2001. Geostatistics – cracks in the foundations? *Earth Science Computer Applications* **16**: 1–3.
- Hopmans JW. 1987. A comparison of various methods to scale soil hydraulic properties. *Journal of Hydrology* **93**: 241–256.

431 Hunt AG. 2005. Continuum percolation theory for saturation dependence of air permeability.
 432 *Vadose Zone Journal* **4**: 134–138. DOI:10.2113/4.1.134.

433 Hunt AG, Ewing RP. 2009. *Percolation Theory for Flow in Porous Media, Lect. Notes Phys.*,
 434 **vol. 771**, 2nd ed., Springer, Berlin.

435 Iversen BV, Moldrup P, Schjønning P, Loll P. 2001. Air and water permeability in differently
 436 textured soils at two measurement scales. *Soil Science* **166**: 643–659.

437 Iversen BV, Moldrup P, Schjønning P, Jacobsen OH. 2003. Field application of a portable air
 438 permeameter to characterize spatial variability in air and water permeability. *Vadose Zone*
 439 *Journal* **2**: 618–626.

440 Iversen BV, Moldrup P, Loll P. 2004. Runoff modelling at two field slopes: Use of in situ
 441 measurements of air permeability to characterize spatial variability of saturated hydraulic
 442 conductivity. *Hydrological Processes* **18**:1009–1026. DOI:10.1002/hyp.1455.

443 Jain P, Powell J, Townsend TG, Reinhart DR. 2005. Air permeability of waste in a municipal
 444 solid waste landfill. *Journal of Environmental Engineering (ASCE)* **131**: 1565–1573.

445 Kabat P, Hutjes RWA, Feddes RA. 1997. The scaling characteristics of soil parameters: from
 446 plot scale heterogeneity to subgrid parameterization. *Journal of Hydrology* **190**: 363–396.

447 Kawamoto K, Moldrup P, Schjønning P, Iversen BV, Komatsu T, Rolston DE. 2006. Gas
 448 transport parameters in the vadose zone: Development and tests of power-law models for air
 449 permeability. *Vadose Zone Journal* **5**: 1205–1215. DOI:10.2136/vzj2006.0030.

450 Kirkham, D. 1947. Field method for determination of air permeability of soil in its undisturbed
 451 state. *Soil Science Society of America Proceedings* **11**: 93–99.

452 Klinkenberg LJ. 1941. The permeability of porous media to liquids and gases. In *Drilling and*
 453 *production practices*: 200–213. American Petroleum Institute, New York.

454 Lipiec J, Hatano R. 2003. Quantification of compaction effects on soil physical properties and
 455 crop growth. *Geoderma* **116**: 107–136.

456 Loll P, Moldrup P, Schjønning P, Riley H. 1999. Predicting saturated hydraulic conductivity
 457 from air permeability: Application in stochastic water infiltration modeling. *Water Resources*
 458 *Research* **35**: 2387–2400.

459 Miller EE, Miller RD. 1956. Physical theory for capillary flow phenomena. *Journal of Applied*
 460 *Physics* **27**: 324–332.

461 Millington RJ, Quirk JM. 1960. Transport in porous media. In *Transactions of 7th International*
 462 *Congress of Soil Science*, Madison, Wisc., U.S.A., edited by Van Beren FA et al., **vol. 1**: 97–
 463 106, Elsevier, Amsterdam.

464 Oliveira LI, Demond AH, Abriola LM, Goovaerts P. 2006. Simulation of solute transport in a
 465 heterogeneous vadose zone describing the hydraulic properties using a multistep stochastic
 466 approach. *Water Resources Research* **42**:W05420. DOI:10.1029/2005WR004580.

467 Peck AJ, Luxmoore RJ, Stolzy JL. 1977. Effect of spatial variability of soil hydraulic properties
 468 in water budget modeling. *Water Resources Research* **13**: 348–354.

469 Poulsen T, Moldrup P, Schjønning P, Massmann J, Hansen J. 1998. Gas permeability and
 470 diffusivity in undisturbed soil: SVE implications. *Journal of Environmental Engineering* **124**:
 471 979–986.

472 Poulsen TG, Iversen BV, Yamaguchi T, Moldrup P, Schjønning P. 2001. Spatial and temporal
 473 dynamics of air permeability in a constructed field. *Soil Science* **166**: 153–162.

474 Rawls WJ, Brakensiek DL, Saxton KE. 1982. Estimation of soil water properties. *Transactions*
 475 *of the American Society of Agricultural Engineers* **25**: 1316–1320.

476 Salvucci G. 1998. Limiting relations between soil moisture and soil texture with implications for
 477 measured, modeled and remotely sensed estimates. *Geophysical Research Letter* **25**: 1757–
 478 1760.

479 Shouse PJ, Mohanty BP. 1998. Scaling of near-saturated hydraulic conductivity measured using
 480 disc infiltrometers. *Water Resources Research* **34**: 1195–1205.

481 Tang AM, Cui YJ, Richard G, Défossez P. 2011. A study on the air permeability as affected by
 482 compression of three French soils. *Geoderma* **162**: 171–181,
 483 DOI:10.1016/j.geoderma.2011.01.019.

484 Tuli A, Kosugi K, Hopmans JW. 2001. Simultaneous scaling of soil water retention and
 485 unsaturated hydraulic conductivity functions assuming lognormal pore-size distribution.
 486 *Advances in Water Resources* **24**: 677–688.

487 Vereecken H, Kasteel R, Vanderborght J, Harter T. 2007. Upscaling hydraulic properties and soil
 488 water flow processes in heterogeneous soils: a review. *Vadose Zone Journal* **6**: 1–28.
 489 DOI:10.2136/vzj2006.0055.

490 Warrick AW, Mullen GJ, Nielsen DR. 1977. Scaling field measured soil hydraulic properties
 491 using a similar media concept. *Water Resources Research* **13**: 355–362.

492 Wu H, Chen T, Wang H, Lu W. 2012. Field air permeability and hydraulic conductivity of
 493 landfilled municipal solid waste in China. *Journal of Environmental Management* **98**: 15–22.

494 Zavattaro L, Jarvis N, Persson L. 1999. Use of similar media scaling to characterize spatial
 495 dependence of near-saturated hydraulic conductivity. *Soil Science Society of America*
 496 *Journal* **63**: 486–492.

497 **List of Figures**

498 Figure 1 The sampling location for Dataset I near Kearney, NE

499 Figure 2 Schematic of the air permeameter used for measuring air permeability in Dataset I

500 Figure 3 Examples of the relationship between saturation degree of air (S_a) and air permeability
501 (k_a) from Dataset I

502 Figure 4 Unscaled and scaled air permeability (k_a) with the reference curves of $k_{a,m}$ for the
503 selected air permeability models from Dataset I: (a) unscaled k_a , (b) scaled k_a for all of the
504 four air permeability models, (c) scaled k_a for the Millington and Quirk (1960) model, (d)
505 scaled k_a for the Hunt (2005) model, (e) scaled k_a for the Brooks and Corey (1964) model,
506 and (f) scaled k_a for the Kawamoto et al. (2006) model

507 Figure 5 Probability plots for the scaling factors obtained from the Hunt (2005) model based on
508 Dataset I

509 Figure 6 Comparison of calculated air permeability (k_a) from the Hunt (2005) model and
510 measured water permeability (k_w) based on Dataset I. The measured saturation degree of air
511 on Day 17 was used to calculate k_a .

512 Figure 7 Unscaled and scaled air permeability (k_a) with the reference curves of $k_{a,m}$ for the
513 selected air permeability models from Dataset II: (a) unscaled k_a , (b) scaled k_a for all of the
514 four air permeability models, (c) scaled k_a for the Millington and Quirk (1960) model, (d)
515 scaled k_a for the Hunt (2005) model, (e) scaled k_a for the Brooks and Corey (1964) model,
516 and (f) scaled k_a for the Kawamoto et al. (2006) model

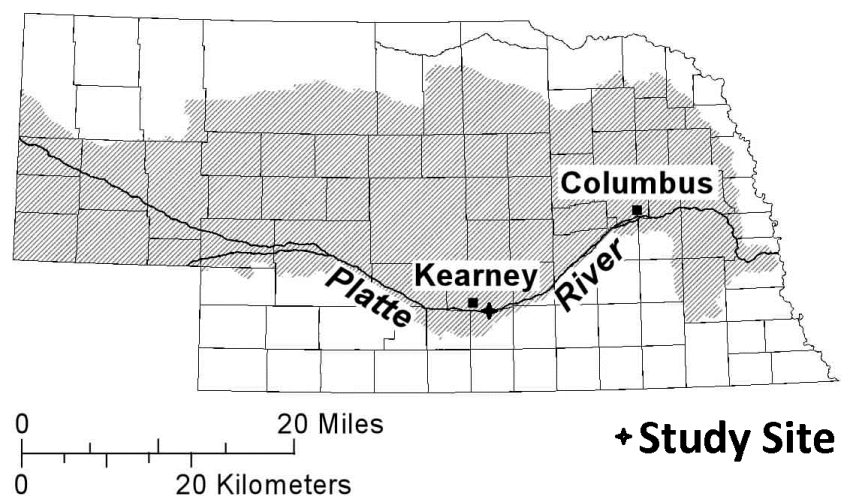


Figure 1 The sampling location for Dataset I near Kearney, NE

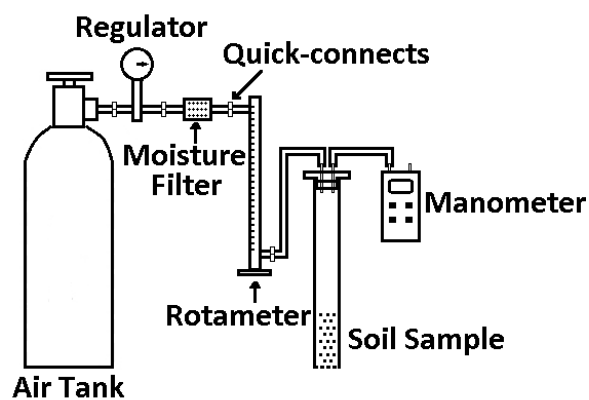


Figure 2 Schematic of the air permeameter used for measuring air permeability in Dataset I

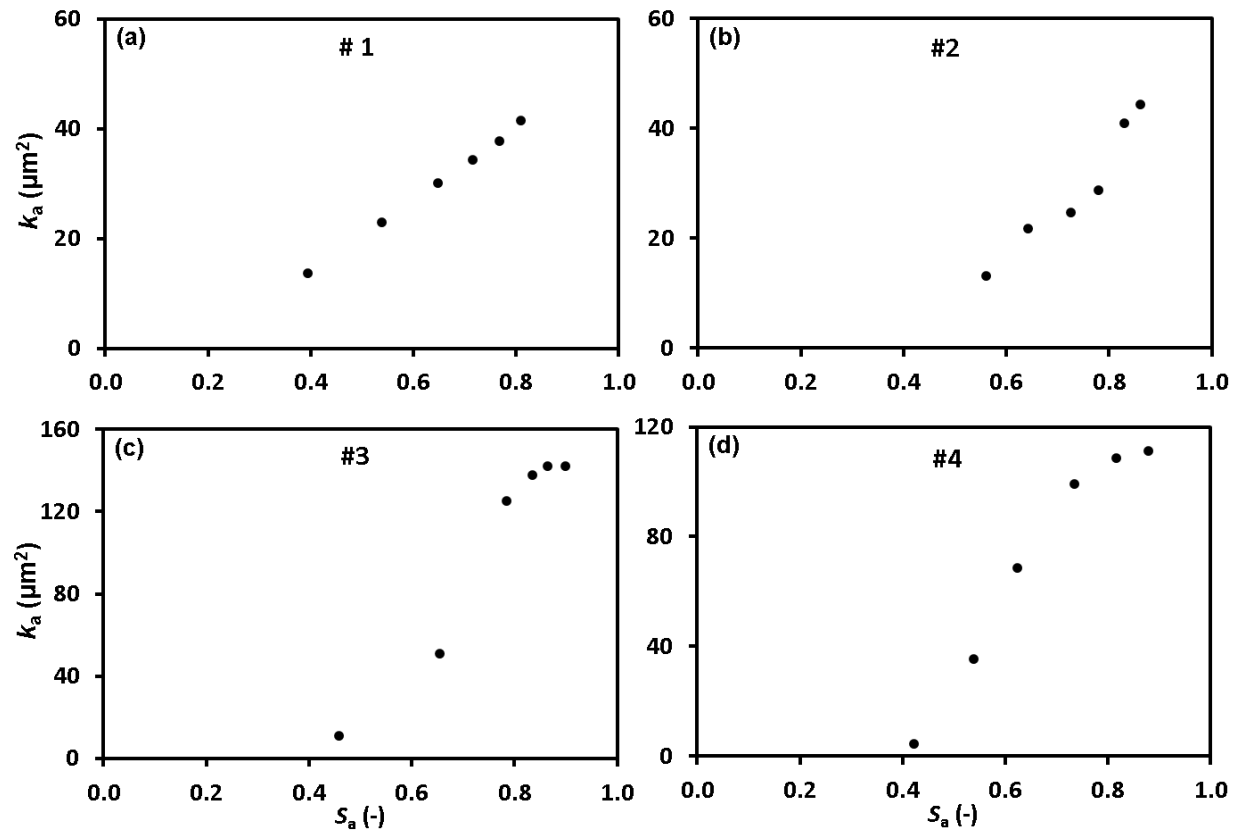


Figure 3 Examples of the relationship between saturation degree of air (S_a) and air permeability (k_a) from Dataset I

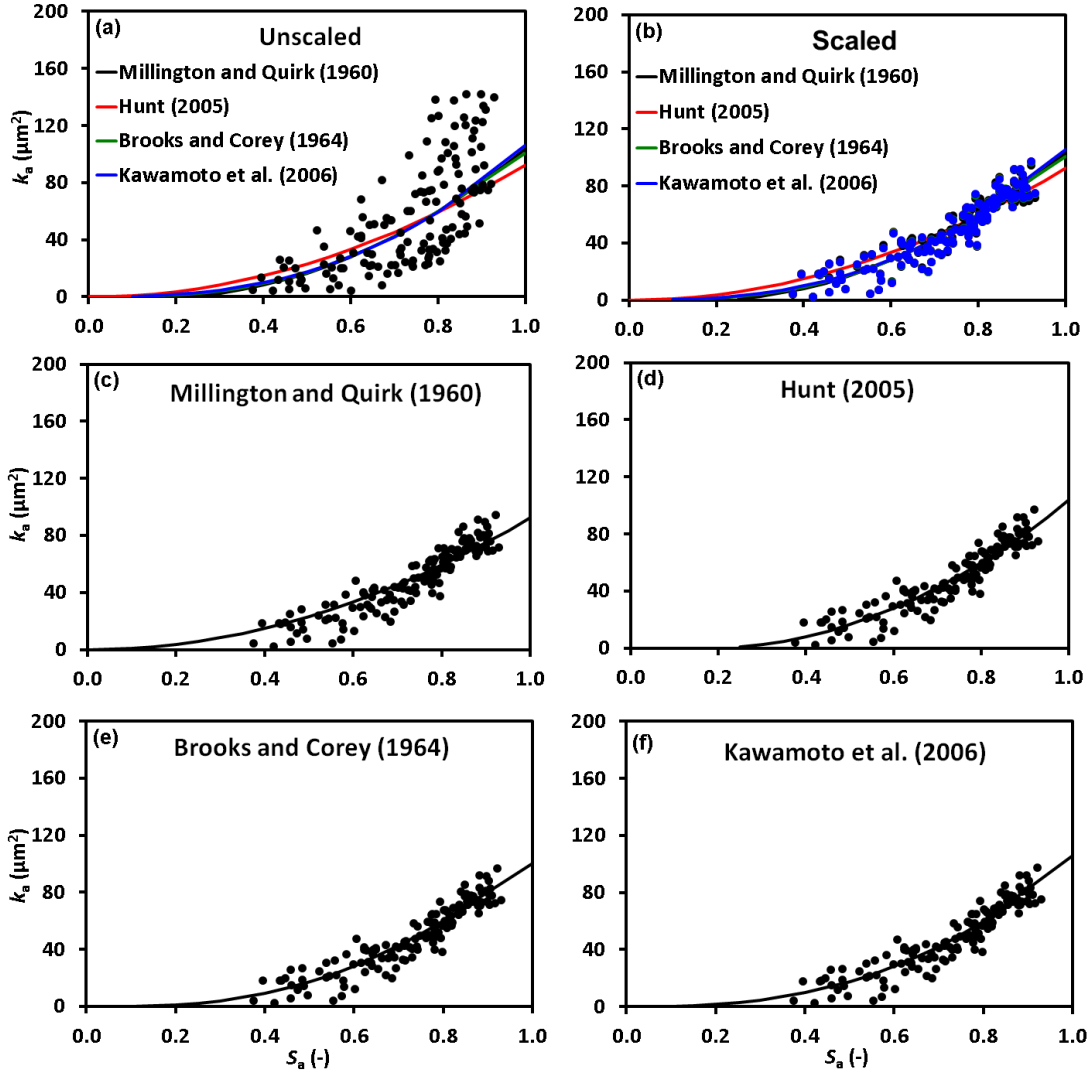


Figure 4 Unscaled and scaled air permeability (k_a) with the reference curves of $k_{a,m}$ for the selected air permeability models from Dataset I: (a) unscaled k_a , (b) scaled k_a for all of the four air permeability models, (c) scaled k_a for the Millington and Quirk (1960) model, (d) scaled k_a for the Hunt (2005) model, (e) scaled k_a for the Brooks and Corey (1964) model, and (f) scaled k_a for the Kawamoto et al. (2006) model

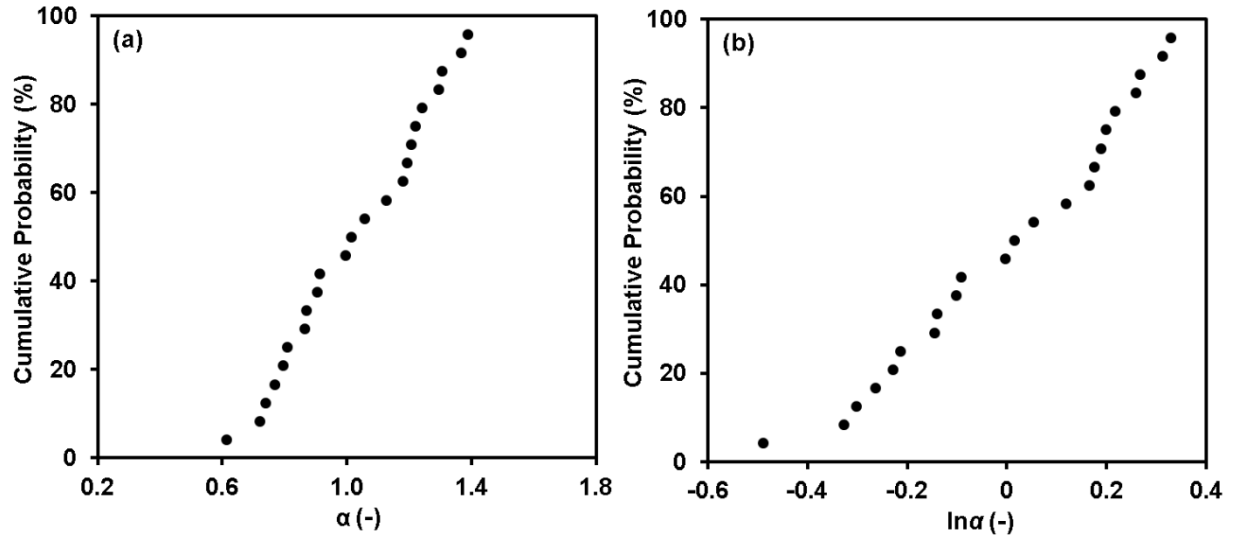


Figure 5 Probability plots for the scaling factors (α_a) obtained from the Hunt (2005) model based on Dataset I

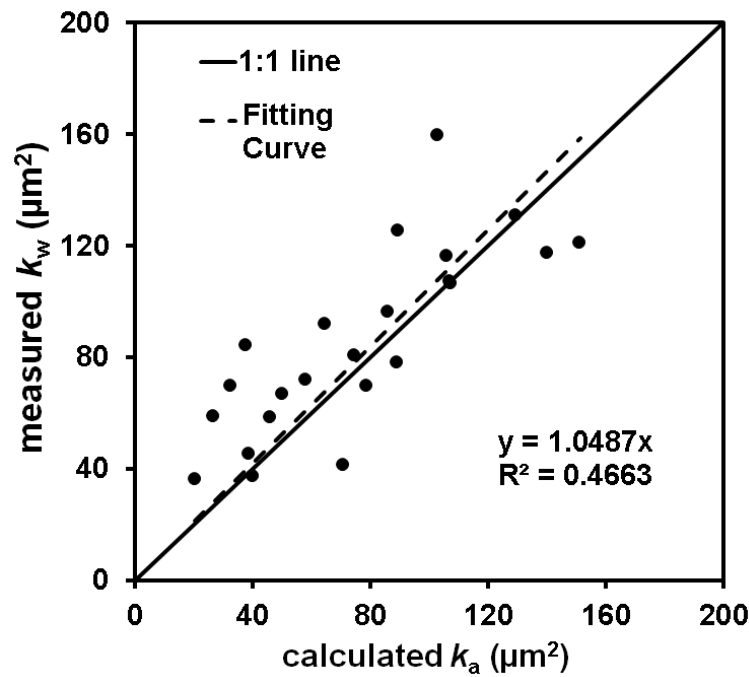


Figure 6 Comparison of calculated air permeability (k_a) from the Hunt (2005) model and measured water permeability (k_w) based on Dataset I. The measured saturation degree of air on Day 17 was used to calculate k_a .

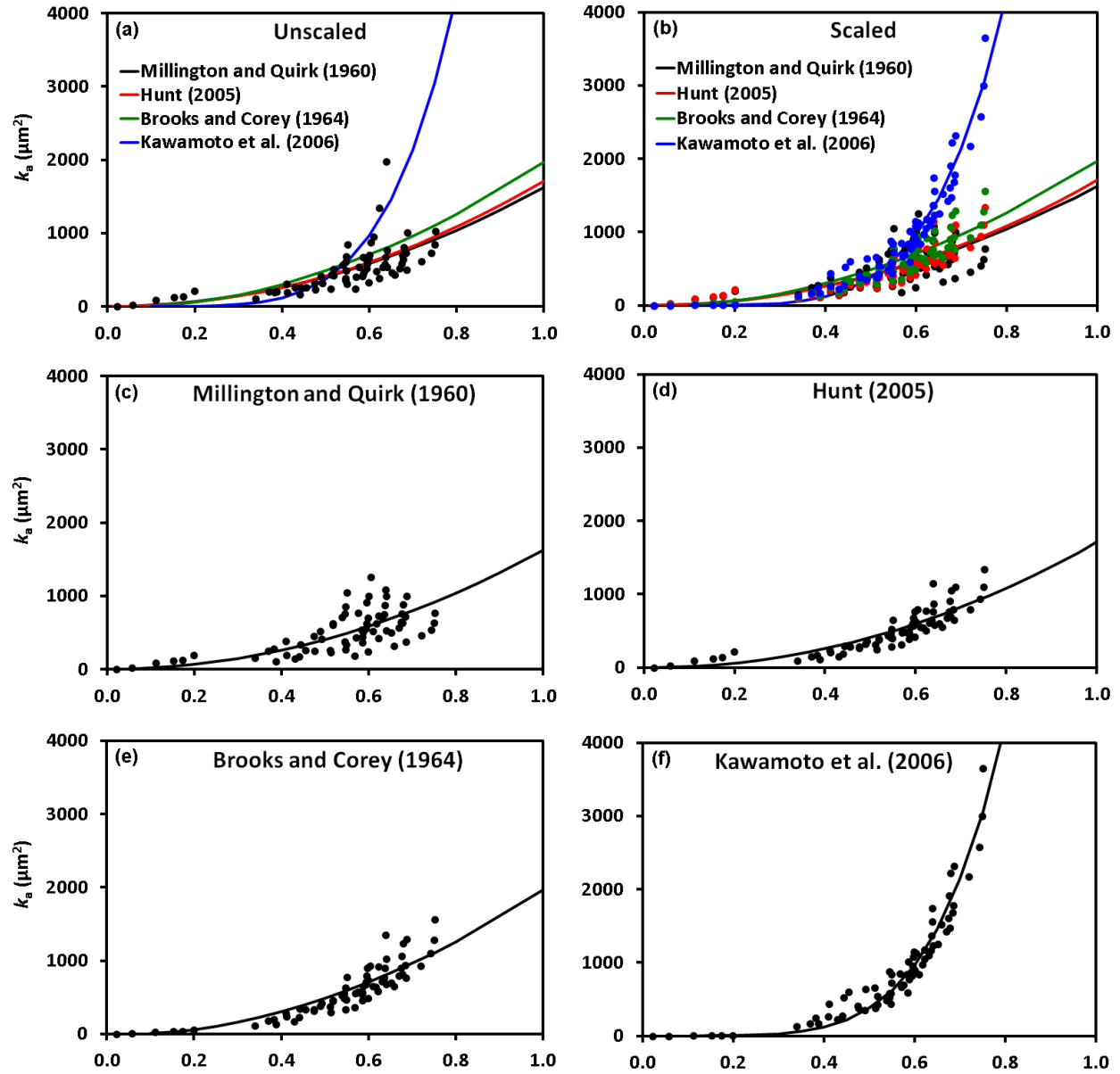


Figure 7 Unscaled and scaled air permeability (k_a) with the reference curves of $k_{a,m}$ for the selected air permeability models from Dataset II: (a) unscaled k_a , (b) scaled k_a for all of the four air permeability models, (c) scaled k_a for the Millington and Quirk (1960) model, (d) scaled k_a for the Hunt (2005) model, (e) scaled k_a for the Brooks and Corey (1964) model, and (f) scaled k_a for the Kawamoto et al. (2006) model

546 **List of Tables**

547 Table 1 Summaries of the physical properties of sediment and soil samples from Dataset I and
548 Dataset II

549 Table 2 Fitting parameters for the reference curves of $k_{a,m}$ with the corresponding RMSE values
550 based on Dataset I

551 Table 2 Fitting parameters for the reference curves of $k_{a,m}$ with the corresponding RMSE values
552 based on Dataset II

Table 1 Summaries of the physical properties of sediment and soil samples from Dataset I and Dataset II

	Dataset I	Dataset II
Texture *	Sand	Sandy Loam
Porosity	0.30	0.52
Gravel (>2mm)	10.9	-
Coarse Sand (2-0.5 mm)	53.0	-
Medium and Fine Sand (0.5-0.05 mm)	36.0	-
Silt and Clay (<0.05 mm)	0.1	-
Sand (2-0.05mm)	-	19.0
Silt (0.002-0.05mm)	-	23.0
Clay (<0.002mm)	-	58.0

* USDA classification

Table 2 Fitting parameters for the reference curves of $k_{a,m}$ with the corresponding RMSE values based on Dataset I

Air Permeability Model	$k_o (\mu m^2)$	$S_{a,t} (-)$	$\gamma (-)$	$\eta (-)$	RMSE	
					Unscaled k_a	Scaled k_a
Millington and Quirk (1960)	92.5	-	-	-	28.4	8.9
Hunt (2005)	103.6	0.168	-	-	27.4	8.0
Brooks and Corey (1964)	100.6	-	3.067	-	33.0	7.8
Kawamoto et al. (2006)	106.0	-	-	1.893	27.4	7.9

Table 3 Fitting parameters for the reference curves of $k_{a,m}$ with the corresponding RMSE values based on Dataset II

Air Permeability Model	$k_o (\mu m^2)$	$S_{a,t} (-)$	$\gamma (-)$	$\eta (-)$	RMSE	
					Unscaled k_a	Scaled k_a
Millington and Quirk (1960)	1625.3	-	-	-	228.7	217.3
Hunt (2005)	1709.4	0.02	-	-	229.5	135.0
Brooks and Corey (1964)	1966.2	-	0.378*	-	257.3	156.7
Kawamoto et al. (2006)	13390.6	-	-	0.724	719.7	188.7

* Taken from Rawls et al. (1982)